

Resident CAPS on dense-core vesicles docks and primes vesicles for fusion

Greg Kabachinski^{†,‡}, D. Michelle Kielar-Grevstad[†], Xingmin Zhang, Declan J. James, and Thomas F. J. Martin^{*}

Department of Biochemistry, University of Wisconsin, Madison, WI 53706

ABSTRACT The Ca²⁺-dependent exocytosis of dense-core vesicles in neuroendocrine cells requires a priming step during which SNARE protein complexes assemble. CAPS (aka CADPS) is one of several factors required for vesicle priming; however, the localization and dynamics of CAPS at sites of exocytosis in live neuroendocrine cells has not been determined. We imaged CAPS before, during, and after single-vesicle fusion events in PC12 cells by TIRF microscopy. In addition to being a resident on cytoplasmic dense-core vesicles, CAPS was present in clusters of approximately nine molecules near the plasma membrane that corresponded to docked/tethered vesicles. CAPS accompanied vesicles to the plasma membrane and was present at all vesicle exocytic events. The knockdown of CAPS by shRNA eliminated the VAMP-2-dependent docking and evoked exocytosis of fusion-competent vesicles. A CAPS(Δ C135) protein that does not localize to vesicles failed to rescue vesicle docking and evoked exocytosis in CAPS-depleted cells, showing that CAPS residence on vesicles is essential. Our results indicate that dense-core vesicles carry CAPS to sites of exocytosis, where CAPS promotes vesicle docking and fusion competence, probably by initiating SNARE complex assembly.

Monitoring Editor

Patrick J. Brennwald
University of North Carolina

Received: Jul 17, 2015

Revised: Dec 12, 2015

Accepted: Dec 18, 2015

INTRODUCTION

Membrane fusion in the multistep endomembrane secretory and endocytic pathways of eukaryotic cells is catalyzed by soluble N-ethylmaleimide sensitive factor-associated protein receptor (SNARE) protein complexes that are assembled by a diverse set of tethering factors cooperating with Sec1/mammalian orthologue of UNC18p (Munc18) proteins (Carr and Rizo, 2010; Yu and Hughson,

2010; Hong and Lev, 2014). Dense-core vesicle (DCV) exocytosis in neuroendocrine cells is a well-studied membrane fusion process that uses the neuronal SNARE proteins syntaxin-1, synaptosomal-associated protein, 25 kDa (SNAP-25), and vesicle-associated membrane protein-2 (VAMP-2; aka synaptobrevin-2; Sollner *et al.*, 1993; Sudhof and Rothman, 2009; Jahn and Fasshauer, 2012). SNARE complex formation during vesicle docking and priming bridges vesicles to the plasma membrane in preparation for Ca²⁺-triggered exocytosis (Wojcik and Brose, 2007; Malsam *et al.*, 2008; Verhage and Sorensen, 2008; Kasai *et al.*, 2012). Although cognate SNARE proteins suffice for docking and fusion of liposomes in vitro (Weber *et al.*, 1998), vesicle docking and priming in cells requires the priming factors calcium-dependent activator protein for secretion (CAPS) and Munc13 (Wojcik and Brose, 2007; Jahn and Fasshauer, 2012; James and Martin, 2013; Imig *et al.*, 2014), as well as Munc18 (Rizo and Sudhof, 2012). The timing and location of SNARE regulators during DCV exocytosis in neuroendocrine cells have been studied to some extent for Munc13 (Friedrich *et al.*, 2013; Kabachinski *et al.*, 2014) and Munc18 (Zilly *et al.*, 2006; Smyth *et al.*, 2010; Smyth *et al.*, 2013; Gandasi and Barg, 2014) but not for CAPS.

CAPS (aka CAPS-1, CADPS, UNC31p) is a neuronal/endocrine-specific protein that reconstitutes Ca²⁺-dependent DCV exocytosis in permeable neuroendocrine cells (Walent *et al.*, 1992;

This article was published online ahead of print in MBoC in Press (<http://www.molbiolcell.org/cgi/doi/10.1091/mbc.E15-07-0509>) on December 23, 2015.

[†]These should be considered as co-first authors.

[‡]Present address: Department of Biology, Massachusetts Institute of Technology, Cambridge, MA 02139.

^{*}Address correspondence to: Thomas F.J. Martin (tfmartin@wisc.edu).

Abbreviations used: BDNF, brain-derived neurotrophic factor; CAPS (aka CADPS), calcium-dependent activator protein for secretion; Munc18, mammalian orthologue of UNC18p; PI(4,5)P₂, phosphatidylinositol 4,5-bisphosphate; SNAP-25, synaptosomal-associated protein, 25 kDa; SNARE, soluble N-ethylmaleimide sensitive factor-associated protein receptor; TIRF, total internal reflection fluorescence; VAMP, vesicle-associated membrane protein.

© 2016 Kabachinski, Kielar-Grevstad, *et al.* This article is distributed by The American Society for Cell Biology under license from the author(s). Two months after publication it is available to the public under an Attribution-Noncommercial-Share Alike 3.0 Unported Creative Commons License (<http://creativecommons.org/licenses/by-nc-sa/3.0>).

“ASCB®,” “The American Society for Cell Biology®,” and “Molecular Biology of the Cell®” are registered trademarks of The American Society for Cell Biology.

Ann *et al.*, 1997). Gene knockouts or RNA interference in flies, worms, mice, or cultured cells indicate that CAPS is essential for DCV exocytosis, specifically at a vesicle priming step (Berwin *et al.*, 1998; Renden *et al.*, 2001; Fujita *et al.*, 2007; Speese *et al.*, 2007; Liu *et al.*, 2008; Speidel *et al.*, 2008; Shinoda *et al.*, 2011; Kabachinski *et al.*, 2014). CAPS is also required for synaptic vesicle priming and docking in neurons (Jockusch *et al.*, 2007; Imig *et al.*, 2014). We showed that CAPS is a SNARE-binding protein (Daily *et al.*, 2010; Khodthong *et al.*, 2011) that promotes SNARE complex formation to accelerate SNARE-dependent liposome fusion (James *et al.*, 2008, 2009). In addition, CAPS binds to phosphatidylinositol 4,5-bisphosphate (PI(4,5)P₂) by a central pleckstrin homology domain, which is required for Ca²⁺-evoked vesicle exocytosis in cells, as well as for CAPS stimulation of SNARE-dependent liposome fusion (Grishanin *et al.*, 2002, 2004; James *et al.*, 2008; Kabachinski *et al.*, 2014). Although these biochemical studies suggest that CAPS operates on the plasma membrane to promote vesicle priming for exocytosis, there is also evidence that CAPS associates with DCVs (Berwin *et al.*, 1998; Grishanin *et al.*, 2002).

The general cytoplasmic distribution of soluble CAPS has precluded studies of membrane-associated CAPS in live cells. The present work localized CAPS in live cells by total internal reflection

fluorescence (TIRF) microscopy and simultaneously monitored evoked DCV exocytosis. CAPS was present in clusters near the plasma membrane that corresponded to docked/tethered DCVs. CAPS arrived at the plasma membrane with DCVs and was present at all exocytic events. Evidence indicated that CAPS functioned from its location on DCVs to promote VAMP-2-dependent DCV docking and priming. It is apparent that DCVs carry resident CAPS to sites of exocytosis to engage plasma membrane effectors for docking and priming.

RESULTS

CAPS localization by TIRF microscopy

CAPS is a soluble protein required for priming DCVs for exocytosis. Because of its cytoplasmic distribution, it had not been possible to detect CAPS association with membranes in live neuroendocrine cells. To determine its localization at sites of exocytosis, we expressed and imaged a CAPS-mKate2 protein in live PC12 cells by TIRF microscopy. In contrast to a soluble fluorescent mKate2 protein, which exhibited a diffuse localization (Figure 1A, top), CAPS-mKate2 localized to clusters within ~160 nm of the coverglass (Figure 1A, bottom). This clustering was similar to that seen by CAPS antibody staining of plasma membrane sheets from PC12 cells

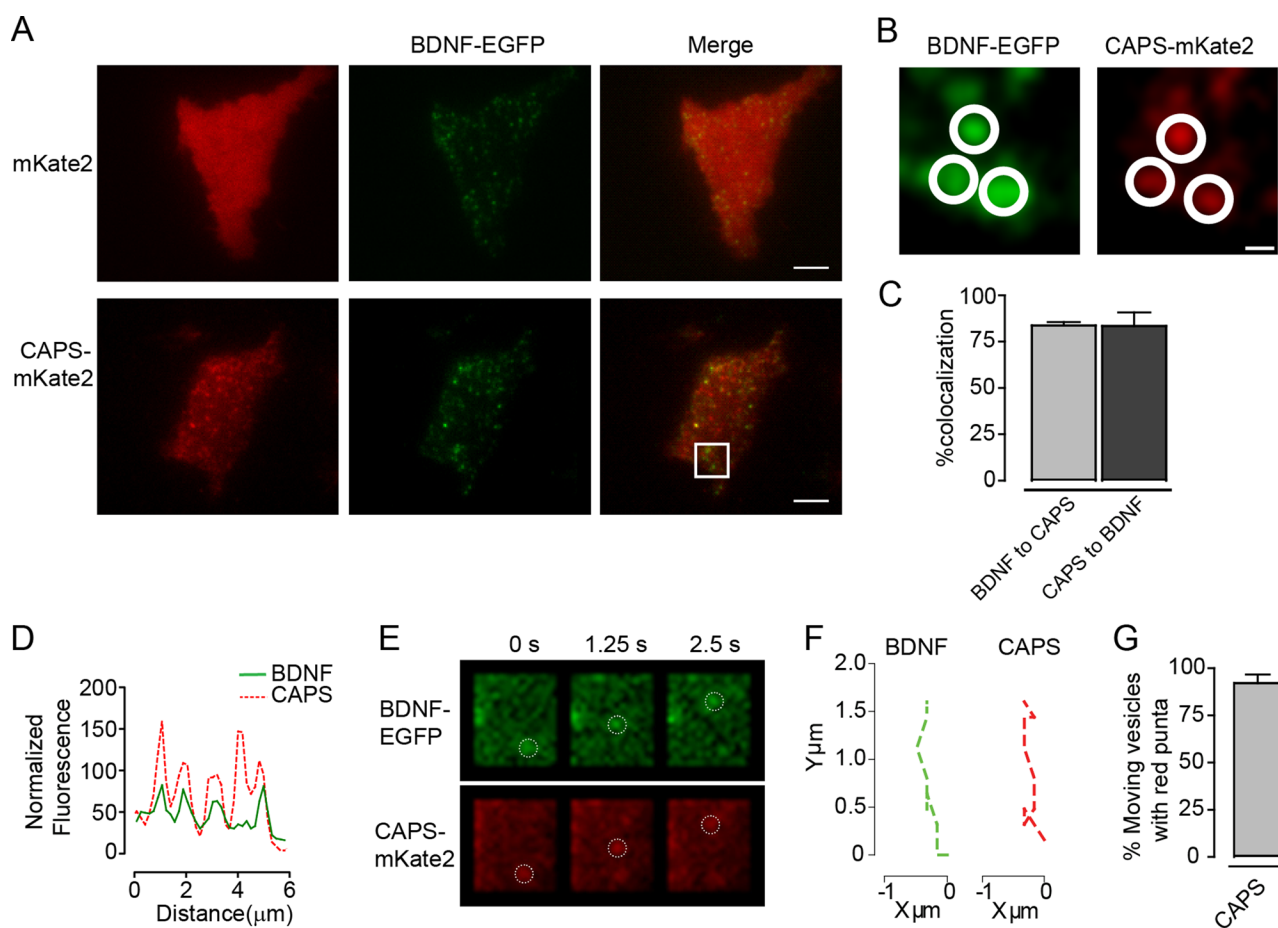


FIGURE 1: Colocalization of CAPS and DCVs in TIRF field. (A) TIRF images of PC12 cells expressing vesicle content BDNF-EGFP (green) and either mKate2 or CAPS-mKate2 (red). Scale bar, 5 μm. (B) Zoomed images are from the area outlined in the white box in A. Scale bar, 400 nm. Closed circles highlight areas of colocalization. (C) Percentage colocalization of DCVs and CAPS. Mean values ± SEM (*n* = 4 cells). (D) Random line scan (10 μm) of merged CAPS/DCV images. (E) TIRF images of moving DCVs (BDNF-EGFP) with CAPS-mKate2. Open circles highlight the moving DCVs in both channels. Scale bar, 1.5 μm. (F) Displacement graph plots trajectories of a moving DCV and a moving CAPS cluster. (G) Graph of percentage of moving DCVs that are associated with a moving cluster of CAPS-mKate2. Mean values ± SEM (*n* = 15–20 vesicles).

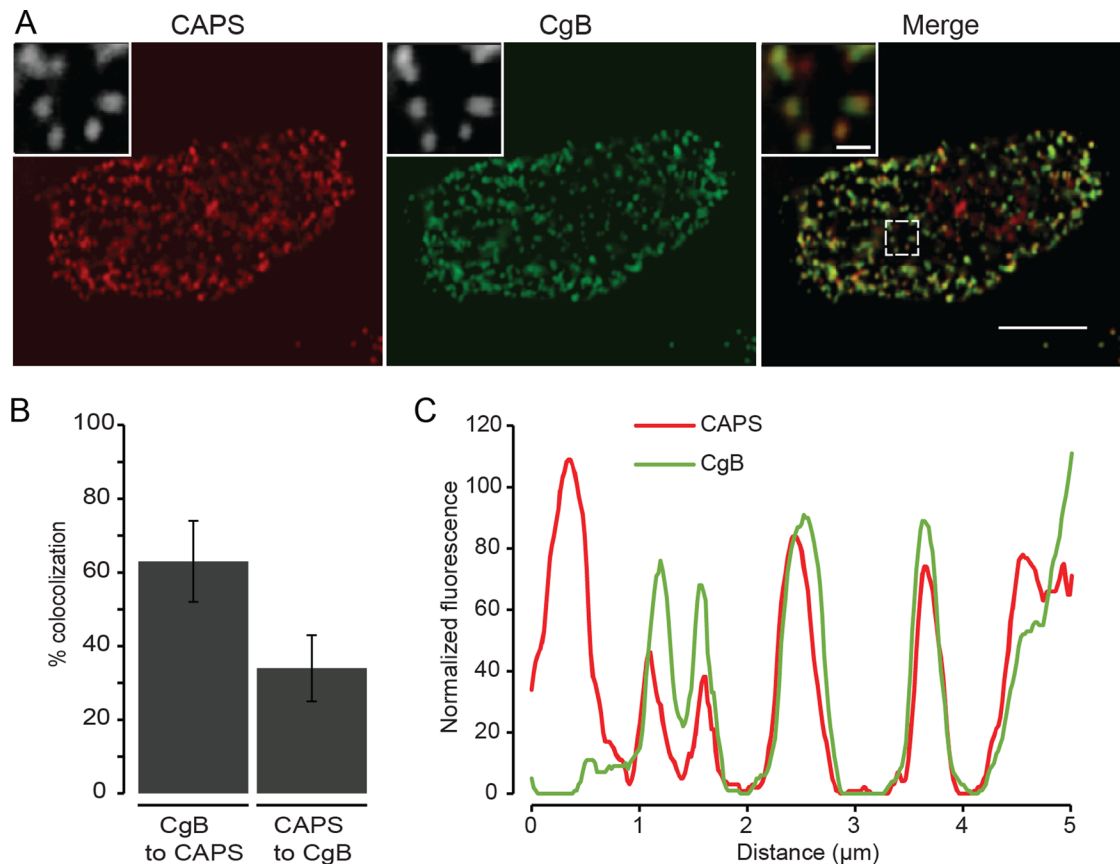


FIGURE 2: Colocalization of endogenous CAPS with chromogranin B-positive DCVs. CAPS (red) and chromogranin B (green) were localized in digitonin-permeabilized, fixed PC12 cells by indirect immunofluorescence by confocal microscopy with z-sectioning. (A) A single section for both channels and a merge. Insets are indicated by a white box. Scale bars, 5 μm (main images), 0.5 μm (insets). (B) Colocalization was assessed across all z-sections using the confined displacement algorithm implemented with the ImageJ GDSC plug-in to provide the Manders coefficients for the stack. Mean values ± SD ($n = 10$ cells). (C) Line scan depicts overall close localization of CAPS with chromogranin B-containing DCVs.

(James *et al.*, 2008). Brain-derived neurotrophic factor (BDNF)-enhanced green fluorescent protein (EGFP) was used as a content marker to monitor the location of DCVs. The distribution of CAPS-mKate2 clusters was similar to that of BDNF-EGFP-containing DCVs at the plasma membrane (Figure 1B). An analysis of colocalization revealed a Manders coefficient of colocalization in both directions (DCV to CAPS cluster and CAPS cluster to DCV) of 0.85 (Figure 1C). This high degree of overlap was also evident in line-scan analyses of images (Figure 1D). We found that CAPS clusters moved with mobile DCVs in the TIRF field, indicating that CAPS is a resident on DCVs (Figure 1, E and G, and Supplemental Movie S1).

To eliminate the possibility that an expressed CAPS-mKate2 protein artificially localized to DCVs, we immunolocalized endogenous CAPS in digitonin-permeabilized cells, which showed that ~63% of DCVs detected by chromogranin B cargo were positive for CAPS (Figure 2, A–C). This estimate from a confocal z-series indicated that most DCVs, and not simply those in proximity to the plasma membrane, had bound CAPS. Whereas CAPS is also a soluble cytosolic protein, the results showed that CAPS is a resident on DCVs, consistent with earlier studies (Berwin *et al.*, 1998; Grishanin *et al.*, 2002).

Number of CAPS molecules on DCVs

Clusters of CAPS are relatively stable in resting cells. About 70% of the original clusters of CAPS persisted at the same sites after 4 min

(Figure 3, A and B). About 70% of the DCVs originally identified also remained in the same position, which suggests that the 30% of CAPS clusters that were no longer present had moved with the corresponding DCVs. Within individual clusters of CAPS, there was little net change in CAPS-mKate2 fluorescence with time, indicating that the steady-state number of CAPS molecules in a cluster on DCVs is relatively fixed (Figure 3C).

Studies of SNARE-dependent liposome fusion suggest that >10 SNARE complexes suffice for fusion (James *et al.*, 2009; Karatekin *et al.*, 2010; van den Bogaart *et al.*, 2010). However, in cells, a larger number of syntaxin-1 molecules (50–75) reside in clusters on the plasma membrane near DCVs, suggesting that only a small subset of SNAREs may be activated for fusion (Sieber *et al.*, 2007; Barg *et al.*, 2010; Knowles *et al.*, 2010). Because DCV-associated CAPS may play a role in inducing SNARE complex assembly, we determined how many molecules of CAPS-mKate2 reside in DCV-associated clusters, using established fluorescence microscopy methods (Coffman and Wu, 2014). Specifically, we counted molecules in TIRF, where signal to noise is high. To eliminate complications from endogenous protein, we reduced CAPS levels by >95% with a short hairpin RNA (shRNA; Figure 3D) that eliminates CAPS activity in DCV exocytosis, and we reexpressed a CAPS-mKate2 protein to fully rescue DCV exocytosis (Kabachinski *et al.*, 2014). Single molecules of CAPS-mKate2 that underwent single-step photobleaching

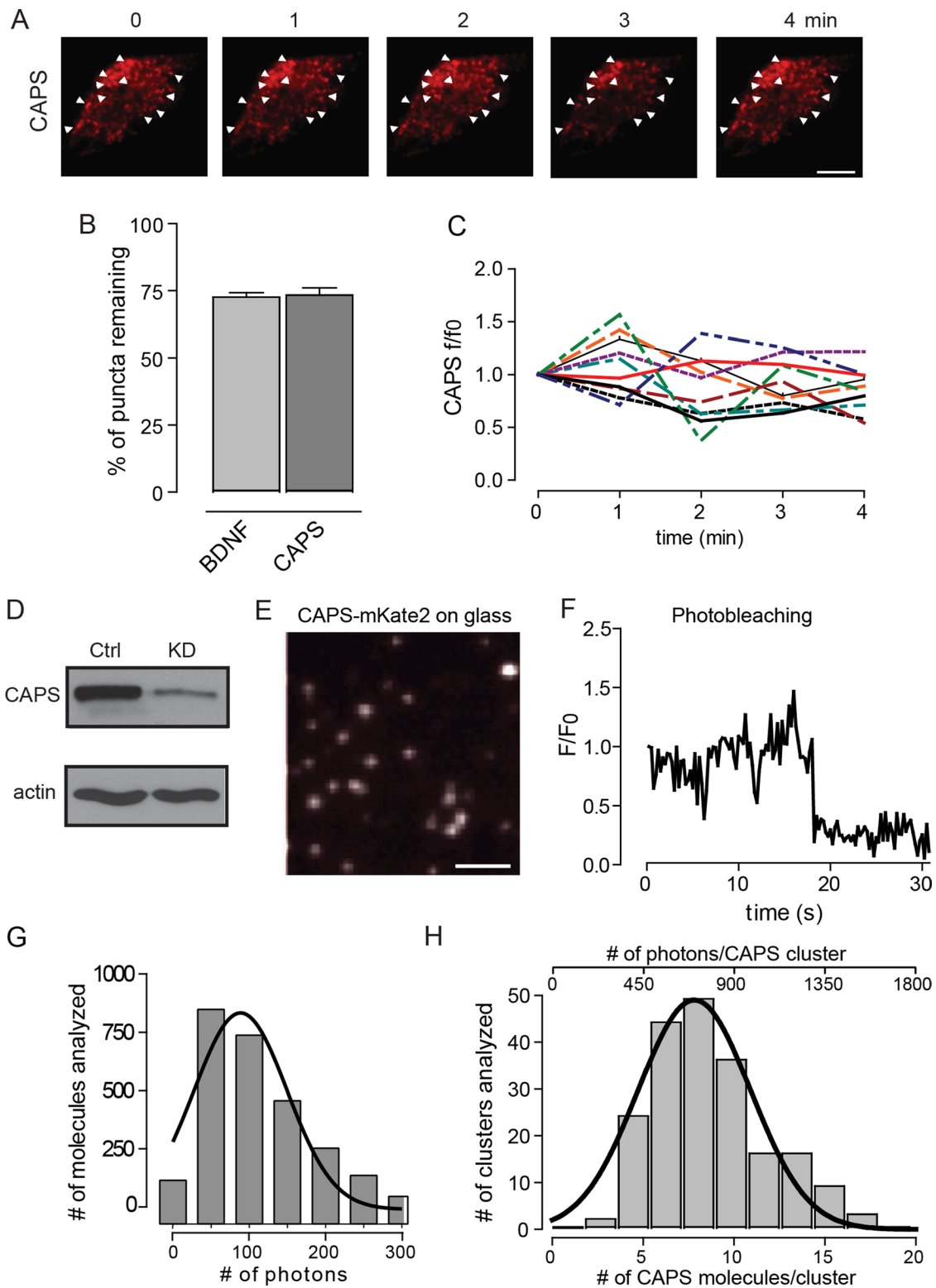


FIGURE 3: Number of CAPS molecules present in clusters. (A) Live PC12 cell expressing CAPS-mKate2 imaged using TIRF in resting buffer for 4 min. White arrowheads point to clusters of CAPS that are present at all times. Scale bar, 5 μ m. (B) Percentage of DCVs and CAPS that remain in the same position after 4 min. (C) Fluorescence intensity changes of 10 random CAPS clusters over the course of 4 min in resting cells. (D) CAPS shRNA was used to knock down CAPS in PC12 cells. (E) TIRF image of cytosol from CAPS-mKate2-expressing HEK cell diluted 1:250,000 and used as intensity standard. Scale bar, 400 nm. (F) Representative photobleaching step of a single CAPS-mKate2 molecule. (G) Histogram of the number of photons emitted by single CAPS-mKate2 molecules. Data were fitted to a single-Gaussian distribution with R -square = 0.91 (n = 2200 single molecules). (H) Histogram of the number of CAPS-mKate2 molecules present in a cluster at the time of fusion (bottom scale) or the photon distribution of clusters with background subtracted (top scale). Data for photons were fitted to a single-Gaussian distribution with R -square = 0.95 (n = 200 events in six cells).

(Figure 3, E and F) were used as a standard. We determined the average integrated fluorescence intensity of molecules within a $0.8\text{-}\mu\text{m}^2$ circle and subtracted average integrated fluorescence intensity in local background corresponding to 89 photons (Figure 3G). Compared to this standard, the mean intensity of CAPS-mKate2 clusters in cells within the same-sized region of interest (ROI; with local background corrected) provided an estimate of 3–18 CAPS molecules resident in clusters, with an average of ~ 9 CAPS molecules/cluster (Figure 3H). This measurement was similar over a 2.5-fold range of CAPS expression (with local background corrected). The range of this estimate is consistent with the size heterogeneity of DCVs (Wang *et al.*, 2003). The results suggest that the number of CAPS molecules on a DCV needed to rescue exocytosis is considerably lower than the number of syntaxin-1 molecules (50–75) in plasma membrane clusters near DCVs in PC12 cells (Sieber *et al.*, 2007; Knowles *et al.*, 2010). If CAPS on DCVs acted stoichiometrically to assemble SNARE complexes, these observations suggest that a small number of SNARE complexes would be formed.

CAPS localization at the time of fusion

The use of TIRF microscopy to image fluorescent cargo-loaded vesicles in real time is a reliable and sensitive method for detecting evoked DCV exocytosis (Steyer and Almers, 2001; Taraska *et al.*, 2003; Kabachinski *et al.*, 2014). The acidic pH of the DCV lumen partially quenches cargo BDNF-EGFP fluorescence, and the rapid increase in fluorescence intensity that occurs upon fusion pore opening in single-vesicle exocytic events serves as a strong signal that exocytosis has occurred. Simultaneous detection of CAPS-mKate2 and BDNF-EGFP fluorescence revealed that virtually all Ca^{2+} -evoked DCV exocytic events occurred at CAPS clusters (Figure 4, A and B).

Several proteins required for vesicle exocytosis were reported to depart from exocytic sites during or after DCV fusion, including complexin and syntaxin-1 (An *et al.*, 2010; Barg *et al.*, 2010). By contrast, under optimal Ca^{2+} stimulation conditions (56 mM KCl), there was usually ($\sim 80\%$) no change in the amount of CAPS present during exocytosis (Figure 4, C and E), but occasionally ($\sim 10\%$) a loss of CAPS was observed (Figure 4, D and E). However, the frequency of exocytic events associated with CAPS dissociation was markedly increased (from 10 to 60%) at stronger depolarization with increased Ca^{2+} influx (95 mM KCl; Figure 4, F–H). Based on the fluorescence profile of BDNF-EGFP, the mode of DCV exocytosis was similar under the two (56 and 96 mM) stimulation conditions (unpublished data). In all cases, CAPS dissociation was restricted to DCVs that underwent exocytosis. CAPS dissociation from DCVs promoted by high Ca^{2+} may be an attenuation mechanism that decreases the probability of fusion pore reopening, but the underlying mechanism is unknown.

Imaging in TIRF identifies evoked vesicle exocytic events from either plasma membrane-associated docked DCVs or newly recruited cytoplasmic DCVs. We previously showed that docked and newly recruited DCVs both require CAPS for exocytosis (Khodthong *et al.*, 2011). Under optimal Ca^{2+} stimulation conditions (56 mM KCl), the majority ($\sim 80\%$) of exocytic events occur from DCVs present at the plasma membrane (Figure 4A), whereas the remaining ($\sim 20\%$) events occur from newly recruited DCVs that become visible in the TIRF field <0.5 s before fusion and quickly transition into fusion (Figure 4I). Both types of DCV fusion events occurred with CAPS clusters present; with fusion events from newly recruited DCVs, CAPS clusters arrived at the plasma membrane with the DCVs (Figure 4, I and J). This confirms that CAPS resides on and travels to the plasma membrane on DCVs.

CAPS is required for docking of DCVs

High ($1\text{ }\mu\text{M}$) concentrations of CAPS promote the stable docking of VAMP-2-containing liposomes onto syntaxin-1/SNAP-25-containing bilayer membranes (James *et al.*, 2009). DCVs have high CAPS surface concentrations (9 molecules/100-nm DCV $\geq 5\text{ }\mu\text{M}$), which could promote DCV docking by assembling SNARE complexes (James *et al.*, 2008, 2009). We tested this idea by determining the molecular requirements for DCV docking/tethering in PC12 cells, using TIRF microscopy. Many of the $\sim 100\text{-nm}$ DCVs in the PC12 cell clone used in these studies are attached to the plasma membrane, based on biochemical and morphological studies (Martin and Kowalchuk, 1997; Fujita *et al.*, 2007; Wu *et al.*, 2012). To circumvent potential fixation artifacts (Verhage and Sorensen, 2008), we used TIRF microscopy in live cells to identify DCVs that were directly tethered or docked to the plasma membrane. We disassembled the cortical actin layer (see *Materials and Methods*), which contains enmeshed DCVs (Lang *et al.*, 2000), and found an immobile (in x, y) pool of DCVs directly attached to the plasma membrane that corresponded to $\sim 65\%$ of the DCVs in our standard TIRF field (Supplemental Figure S1A). This pool of DCVs was strongly reduced by the knockdown of syntaxin-1 and SNAP-25 (Supplemental Figure S1B), consistent with DCVs being in a tethered or docked state (Wu *et al.*, 2012; Mohrmann *et al.*, 2013).

Previous studies showed that the total number of DCVs in the TIRF field was unchanged by CAPS depletion (Khodthong *et al.*, 2011; Nojiri *et al.*, 2009), and we confirmed this finding for the immobile (in x, y) DCV pool. However, CAPS depletion might affect transitions between tethered and docked DCVs, both of which are visible in the TIRF field. DCVs that are tightly docked to the plasma membrane can be distinguished from more loosely tethered vesicles by monitoring vesicle movement in the axial z -dimension (Toonen *et al.*, 2006; Karatekin *et al.*, 2008). To measure apparent vesicle attachment lengths in the z -dimension, we calculated the maximum z -displacement of individual DCVs from the minimal and maximal fluorescence of BDNF-EGFP (see Supplemental Figure S2A and *Materials and Methods*). The normalized z -movement distribution of 487 attached vesicles in 25 cells (Figure 5, A and B) was best fitted by three Gaussian curves with means centered at $\sim 28, 42,$ and 55 nm , respectively (Figure 5C). By contrast, the z -movement of immobilized beads fitted to a single Gaussian with a mean centered at 27 nm (Supplemental Figure S2, B and C). The results suggest that DCV attachment to the plasma membrane is mediated through different molecular complexes that can be reliably classified by z -movement lengths. The majority ($\sim 70\%$) of DCVs in the TIRF field resided in the shortest attachment group (Figure 5C, pool 1), which we refer to as tightly docked, whereas the remaining ($\sim 30\%$) DCVs were distributed into two longer attachment groups, which we refer to collectively as tethered (Figure 5C, pools 2 and 3).

CAPS knockdown reduced the number of tightly docked DCVs (pool 1) by $\sim 40\%$ (Figure 5, D and E). Because the total number of immobile (in x, y) DCVs in the TIRF field was unchanged upon CAPS knockdown, there was a corresponding increase in the number of tethered DCVs (pools 2 and 3) to $\sim 60\%$ of the total population from $\sim 30\%$ in wild-type cells ($n = 645$ vesicles from 25 cells, $p < 0.0001$; Mann–Whitney test and two-way analysis of variance [ANOVA]; Figure 5E). Unlike the effect of CAPS depletion, the depletion of *ubMunc13-2*, a priming factor that is cytoplasmic in resting PC12 cells (Kabachinski *et al.*, 2014), did not significantly affect the distribution of z -movements (Figure 5, D and E; $n = 195$ from nine cells, $p > 0.05$; Mann–Whitney test).

The effect of VAMP-2 depletion was strikingly similar to that for CAPS knockdown. VAMP-2 depletion had little effect on the total

number of immobile (in x , y) DCVs in our standard TIRF field (Supplemental Figure S1B) but shifted tightly docked DCVs to a tethered state as measured in the z -dimension (Figure 5, F and G), similar to the effect of CAPS depletion (Figure 5E). As a control for the effect of VAMP-2 knockdown, the knockdown of syntaxin-1 and -9, the major functional synaptotagmin isoforms in PC12 cells (Lynch and Martin, 2007), had no detectable effect on DCV docking or tethering (Figure 5G). Our results suggest that CAPS and VAMP-2 share a common pathway for DCV docking. Indeed, the depletion of both CAPS and VAMP-2 had the same effect on vesicle z -movement distribution as single depletion (Supplemental Figure S2D), which is consistent with both proteins acting in a common pathway. The simplest interpretation of these data is that ~40% of tightly docked DCVs are attached by VAMP-2-containing SNARE complexes formed in a CAPS-dependent process.

To further distinguish between tightly docked and tethered DCVs and determine whether CAPS- and VAMP-2-dependent docking can be detected as a decrease in net vesicle distance from the coverglass, we altered the penetration depth of the TIRF field and acquired images at penetration depths of ~90, ~130, and >130 nm (see *Materials and Methods*). There was a significant increase in the number of DCVs (0.57 ± 0.05 to 0.83 ± 0.06 vesicle/ μm^2 ; $n = 31$ cells) as the penetration depth was increased from 90 to 130 nm (Figure 6, A–C). This result confirmed that in wild-type cells, the majority of DCVs are tightly docked, whereas the remaining DCVs are tethered at longer distances. Depletion of CAPS (Figure 6B) or VAMP-2 (Figure 6C) resulted in a significant reduction in the DCV density when the penetration depth was 90 nm compared with wild-type cells but not when the penetration depth was ≥ 130 nm. This suggests that CAPS and VAMP-2 are required for the tight docking of a subset of DCVs that are tethered at longer distances in the absence of these proteins.

Resident CAPS on DCVs functions in docking and exocytosis

The detection of distinct DCV attachment states (docked vs. tethered) in live cells by TIRF microscopy allowed us to assess the fusion competence of DCVs by depolarizing the cells to promote Ca^{2+} influx. In a time course, most exocytic events evoked by depolarization occurred within 3 min (Figure 7F). We found that the fraction of attached DCVs in wild-type cells that underwent exocytosis within 3 min was 33%, which we expressed as a fusion probability of 0.33 (Figure 7A). The fusion-competent DCVs may correspond in part to the DCVs that depend on VAMP-2 and CAPS for docking (Figure 5). Indeed, the depletion of CAPS, VAMP-2, or syntaxin-1 and SNAP-25 strongly reduced fusion probabilities (Figure 7A). This suggests that the subset of DCVs that are fusion competent formed SNARE-containing docking complexes in a process dependent on CAPS.

CAPS is present on DCVs and could interact with plasma membrane constituents at the time of DCV arrival at the plasma membrane. To determine whether CAPS function requires its residence on DCVs, we used a CAPS(ΔC135) protein that lacks a C-terminal vesicle-binding domain (Grishanin *et al.*, 2002). In CAPS-depleted cells, an expressed CAPS(ΔC135)-mKate2 protein did not localize to membrane-proximal clusters corresponding to docked/tethered DCVs (Figure 7, B and C). To determine whether CAPS(ΔC135) was functionally active, we tested whether it would rescue DCV docking in cells depleted of CAPS. The reduced number of tightly docked DCVs in resting cells depleted of CAPS was rescued by reexpression of wild-type CAPS (Figure 7, D and E). In contrast, expression of CAPS(ΔC135) failed to restore the number of tightly docked DCVs to wild-type levels, and the number of tethered DCVs remained similar to that in CAPS-depleted cells (Figure 7, D and E). That

CAPS(ΔC135) failed to promote tight docking indicates that resident CAPS on DCVs is required for DCV docking.

To determine whether CAPS(ΔC135) was functionally active in evoked vesicle exocytosis, we monitored the number of exocytic events in stimulated cells. The number of exocytic events in stimulated cells was strongly reduced by CAPS knockdown compared with wild-type cells (Figure 7F) and was restored by reexpression of wild-type CAPS (Figure 7G). In contrast, expression of CAPS(ΔC135) failed to restore evoked exocytosis (Figure 7G). The results indicate that CAPS residence on DCVs is essential for its function in promoting DCV fusion competence.

DISCUSSION

SNARE proteins on the vesicle and plasma membrane assemble into complexes during the vesicle-docking and -priming reactions that precede Ca^{2+} -triggered fusion (Xu *et al.*, 1998; Sorensen *et al.*, 2006; Weninger *et al.*, 2008; Takahashi *et al.*, 2010; Kasai *et al.*, 2012; Imig *et al.*, 2014). CAPS plays a key role in vesicle priming and promotes SNARE complex formation *in vitro* (James *et al.*, 2009). However, the location and dynamics of CAPS at sites of exocytosis in live cells had not been determined. The present work clarifies the DCV priming process in neuroendocrine cells by showing that CAPS is a resident on DCVs that functions to promote docking and fusion competence.

Because CAPS is an abundant cytoplasmic protein, its localization on membranes in live cells was difficult to study. In the present work, TIRF microscopy revealed that CAPS clusters at the plasma membrane correspond to docked/tethered DCVs. The CAPS clusters moved with mobile DCVs and arrived at the plasma membrane with DCVs. We also found that DCVs throughout permeabilized cells contain resident CAPS, consistent with earlier work (Berwin *et al.*, 1998; Grishanin *et al.*, 2002). This differs from a recent report on hippocampal neurons, in which CAPS localized to synaptic regions but was not detected on mobile DCVs (Farina *et al.*, 2015). We attribute this difference to the higher signal-to-noise detection of TIRF microscopy in our studies, in which clusters of approximately nine molecules of CAPS on DCVs were detected. Consistent with finding CAPS as a resident on DCVs, previous studies showed that CAPS regulates catecholamine uptake by DCVs in chromaffin cells (Speidel *et al.*, 2005; Liu *et al.*, 2008; Brunk *et al.*, 2009), implying an interaction between CAPS and DCVs. The identity of proteins and/or lipids on DCVs that CAPS binds remains to be determined.

The number of CAPS molecules on DCVs was regulated under specific conditions. CAPS clusters on DCVs did not change substantially when exocytosis occurred under optimal Ca^{2+} influx conditions. However, greater Ca^{2+} influx, while not altering the number of exocytic events or the cavicapture mode of fusion (Kabachinski *et al.*, 2014), promoted the dissociation of CAPS at the time of fusion pore opening. This could represent a Ca^{2+} -dependent desensitization mechanism that decreases the probability of a second fusion pore opening in the cavicapture mode (Harata *et al.*, 2006; MacDonald *et al.*, 2006; Llobet *et al.*, 2008; Xia *et al.*, 2009). The nature of the Ca^{2+} - and exocytosis-dependent process responsible for CAPS dissociation is unknown but may be related to the strong stimulus-triggered translocation of CAPS from synaptic regions recently described for hippocampal neurons (Farina *et al.*, 2015).

Our studies identified a functional role for DCV-resident CAPS in promoting docking and fusion competence. We describe a TIRF-based assay to assess DCV attachment to the plasma membrane in live PC12 cells. Corrections for movement and elimination of actin associations revealed one major and two minor pools of plasma membrane-attached DCVs. Immobile (in x , y) DCVs in the TIRF field

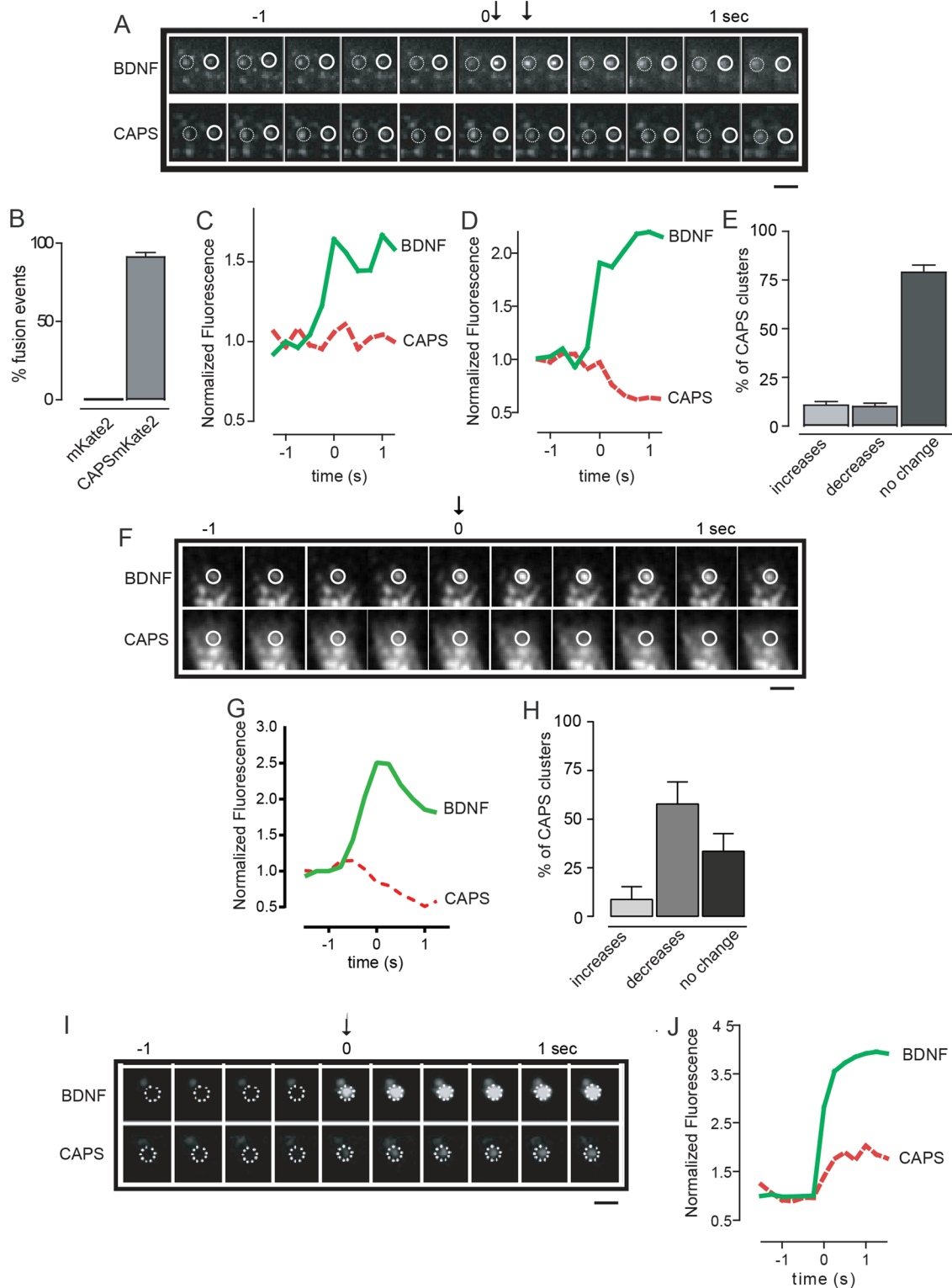


FIGURE 4: CAPS localization during DCV exocytosis. (A) Exocytosis was stimulated by depolarization with 56 mM KCl, and two separate fusion events were imaged by TIRF at 4 Hz. BDNF-EGFP exhibited increased fluorescence at the time of fusion pore opening (arrows). CAPS-mKate2 was imaged simultaneously. The first fusion event is indicated by the closed circle and the second event by the open circle; the time bar (in seconds) shows $t = 0$ for the first fusion event and arrows for both events. Scale bar, 2 μm . (B) Histogram shows the percentage of DCV fusion events ($\pm\text{SEM}$, $n = 110$) that occurred with a CAPS-mKate2 cluster. Soluble mKate2 was expressed as a control in separate cells. (C) Fluorescence intensity profiles of BDNF-EGFP (green) and CAPS-mKate2 (red) corresponding to the open circles in A. The fluorescence intensity of the CAPS-mKate2 cluster associated with this fusion event did not change. (D) Fluorescence intensity profiles of BDNF-EGFP (green) and CAPS-mKate2 (red) corresponding to the closed circles in A. The CAPS-mKate2 cluster associated with this fusion event decreased during fusion. (E) Multiple events similar to those in C and D

that exhibited short attachments were termed tightly docked, whereas those with longer attachments were termed tethered. These were distinguished by both z-dimension movement and net distances from the coverglass. A subset of the tightly docked DCVs were fusion competent and likely attached by VAMP-2 interactions with syntaxin-1/SNAP-25 complexes. Previous studies in chromaffin and PC12 cells documented small pools of DCVs attached via VAMP-2 (Nofal *et al.*, 2007; Wu *et al.*, 2012). In cells depleted of VAMP-2 or CAPS, this subset of tightly docked DCVs shifted to a tethered state, which lost competence for evoked fusion. These findings indicate that CAPS is required to convert DCVs from a tethered to a docked state. The DCV tether was not defined in our studies but may correspond to rabphilin-3, a positive-acting tether for DCVs in PC12 cells (Tsuboi and Fukuda, 2005; Larson *et al.*, 2014).

There are multiple mechanisms for tethering and docking DCVs, with some leading to fusion incompetence (Gomi *et al.*, 2005; Tsuboi and Fukuda, 2006; Hugo *et al.*, 2013). The VAMP-2-, CAPS-dependent pathway identified here leading to fusion competence may be a minor component in cells in which only a small fraction of docked DCVs undergo evoked fusion. Reduced DCV docking upon CAPS depletion has been reported for some neural or neuroendocrine cells, using rapid-freeze or conventional electron microscopy or live-cell TIRF methods (Zhou *et al.*, 2007; Hammarlund *et al.*, 2008; Speidel *et al.*, 2008; Lin *et al.*, 2010; Sadakata *et al.*, 2013; Imig *et al.*, 2014). However, studies in some systems did not detect such changes, which may be attributed to the methods used or to the small size of a CAPS-dependent pool of docked DCVs (Fujita *et al.*, 2007; Jockusch *et al.*, 2007; Liu *et al.*, 2008; Farina *et al.*, 2015).

We propose that transitions of tethered DCVs to a tightly docked state is mediated by CAPS acting to promote the formation of SNARE complexes. In a reconstituted system, CAPS promoted the stable docking of VAMP-2-containing liposomes onto supported bilayers containing syntaxin-1/SNAP-25 heterodimers (James *et al.*, 2009). CAPS promotion of VAMP-2-dependent DCV docking may be only one step in the overall DCV priming process that renders DCVs fusion competent in PC12 cells. The Ca²⁺-dependent recruitment of ubMunc13-2 is also required for DCV exocytosis in PC12 cells (Kabachinski *et al.*, 2014), and yet we found that the knock-down of ubMunc13-2 did not affect the tightly docked DCV pool in resting cells. These results suggest that CAPS promotes SNARE complex assembly that is sufficient for DCV docking but not full priming. CAPS may promote the formation of a limited number of SNARE complexes that suffice for docking but not for fusion (Shi *et al.*, 2012). Alternatively, SNARE complexes assembled by CAPS could be only N-terminally zippered (Sorensen *et al.*, 2006) and require the action of other factors such as ubMunc13-2 to promote full priming. Direct studies of SNARE complex formation on the subset of tightly docked, fusion-competent DCVs will be needed to assess these possibilities.

DCV docking and priming would be efficiently promoted by concentrated resident CAPS on DCVs. A CAPS(Δ C135) protein that failed to localize to DCVs was incapable of promoting tight docking of DCVs or the promotion of fusion competence. The CAPS(Δ C135) protein is likely properly folded because it exhibits activity in permeable cell assays at higher concentrations (Grishanin *et al.*, 2002). Overall these studies indicate that CAPS residence on DCVs is required for CAPS function in DCV exocytosis. High concentrations of CAPS on DCVs could function *in-trans* in low-affinity interactions with the plasma membrane effectors PI(4,5)P₂ and syntaxin-1/SNAP-25. CAPS is effective in solution at micromolar concentrations in stimulating SNARE-dependent liposome fusion without latency (James *et al.*, 2008, 2009), suggesting that CAPS could initiate SNARE complex formation upon arrival of DCVs at the plasma membrane. Previous studies showed that CAPS depletion eliminates the fusion of both docked and newly recruited DCVs (Khodthong *et al.*, 2011). The present work helps to explain how newly recruited DCVs with the resident priming factor CAPS could undergo rapid exocytosis (crash fusion) in stimulated cells (Kasai *et al.*, 2012).

In summary, this work shows that CAPS is a peripherally bound resident protein on DCVs and is present at all sites of DCV exocytosis. Resident DCV-bound CAPS is essential for the docking and fusion competence of DCVs. This indicates that DCVs carry priming factors to sites of exocytosis at the plasma membrane. That the priming factor CAPS promotes docking of DCVs contributes to the emerging view (Imig *et al.*, 2014) that vesicle docking and priming are overlapping rather than distinct steps involving the assembly of SNARE complex intermediates.

MATERIALS AND METHODS

DNA constructs

The plasmid encoding BDNF-EGFP was provided by V. Lessmann (Johannes Gutenberg Universität, Mainz, Germany). The botulinum neurotoxin (BoNT) E light chain expression plasmid was previously described (Zhang *et al.*, 2002). The plasmids encoding BoNT C1 light chain and tetanus toxin (TeTx) light chain were provided by J. Blasi (University of Barcelona, Barcelona, Spain). Synaptotagmin 1 expression plasmids were previously described (Lynch and Martin, 2007). shRNA vectors for the down-regulation of Syx1a were constructed in the ExpressionArrest pSM2 vector (Open Biosystems, Huntsville, AL) with 22-mers that target nucleotides 591–612 of Syx1a, using designs based on described methods (Paddison *et al.*, 2004). All constructs were checked by sequencing. shRNA plasmids targeting rat isoforms of synaptotagmin-1 and -9 and SNAP-25b were previously described (Aikawa *et al.*, 2006; Lynch and Martin, 2007).

The plasmid CAPS-mKate2 was generated by subcloning rat CAPS from a CAPS-myc-his pcDNA3.1 plasmid into pmKate2-N1 from Evrogen using XhoI and KpnI. There is a 23-amino acid linker between CAPS and mKate2 (EFHHTGLVDPSSVPRAR-DPPVAT). A glutathione S-transferase–rat Munc18-1 plasmid was used as a

were scored for changes in CAPS-mKate2 fluorescence (by >15%) and plotted as increased, decreased, or unchanged after exocytosis stimulated at 56 mM KCl (\pm SEM, $n = 110$). (F) Exocytosis was stimulated by depolarization with 95 mM KCl, and single fusion events were imaged by TIRF at 4 Hz. Time bar (in seconds) shows $t = 0$ for fusion pore opening. Scale bar, 2 μ m. At stronger depolarization, fusion events were frequently accompanied by a decrease in CAPS-mKate2 fluorescence. (G) Fluorescence intensity profiles of BDNF-EGFP (green) and CAPS-mKate2 (red) corresponding to the fusion event in F, showing decrease in CAPS-mKate2 fluorescence. (H) Histograms show the percentage of DCV fusion events stimulated by 95 mM KCl that occurred with CAPS-mKate2 fluorescence increasing or decreasing (by >15%) or remaining unchanged (\pm SEM, $n = 58$). (I) Arrival of a new DCV (BDNF-EGFP) at the plasma membrane (indicated as $t = 0$ with arrow) in a cell stimulated at 56 mM KCl. Imaging by TIRF at 4 Hz with simultaneous imaging of CAPS-mKate2. Scale bar, 2 μ m. (J) Representative fluorescence intensity profile of BDNF-EGFP (green) and CAPS-mKate2 (red) during DCV arrival at the plasma membrane, showing simultaneous arrival of CAPS.

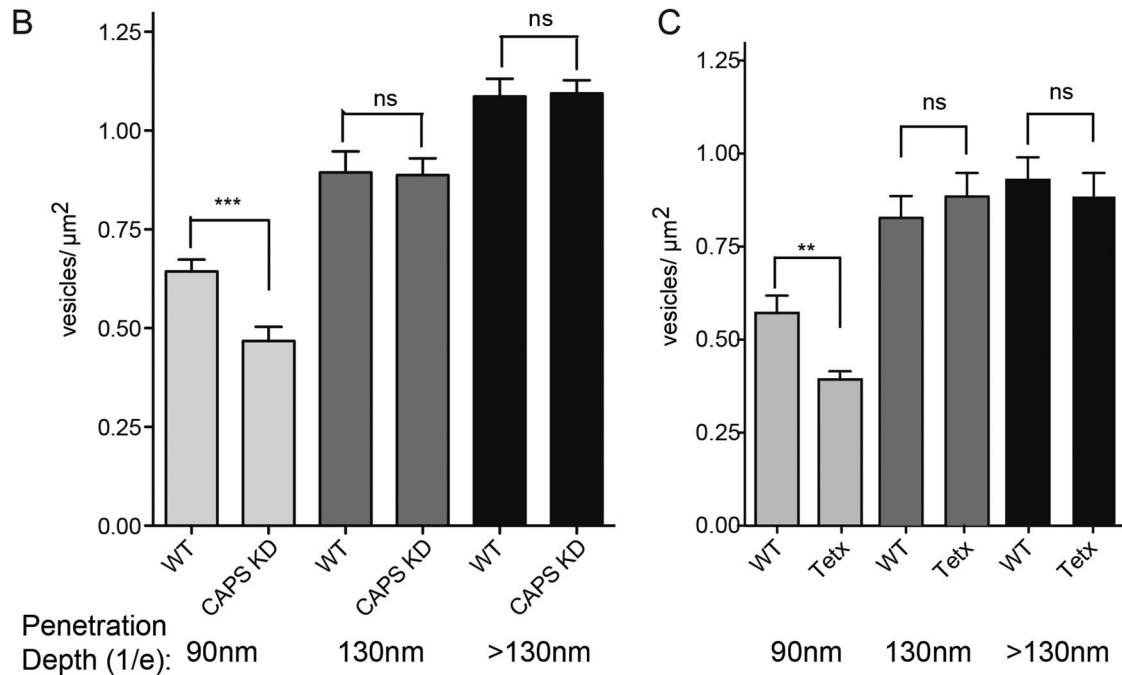
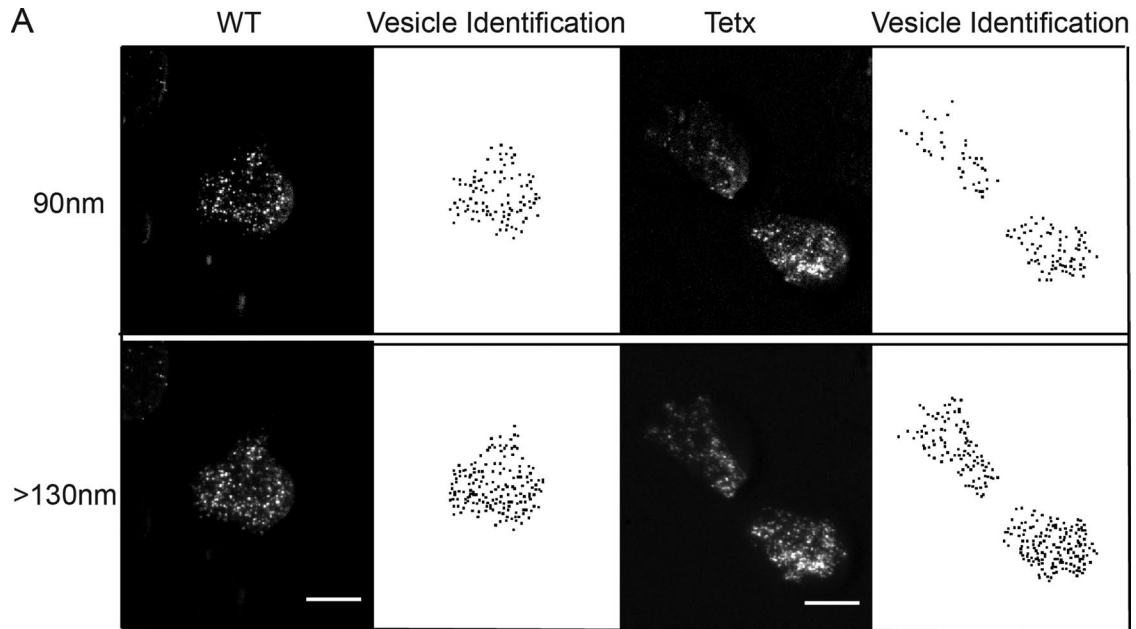


FIGURE 6: Direct imaging of pools of attached DCVs in PC12 cells. (A) Representative image of wild-type or tetanus toxin light chain-expressing PC12 cell with BDNF-EGFP as DCV cargo imaged at TIRF angles corresponding to $1/e$ values of 90 or >130 nm (scale bar, 5 μ m). Vesicle density was calculated from the binary images created through identification of local maxima above a background noise tolerance. (B) Quantitation of DCV density of wild-type or CAPS knockdown cells at penetration depths of 90, 130, and >130 nm (means \pm SE, $n \geq 22$ cells, *** $p < 0.001$). (C) Quantitation of DCV density of wild-type or tetanus toxin light chain-expressing cells at penetration depths of 90, 130, and >130 nm (means \pm SE, $n \geq 25$ cells; ** $p \leq 0.01$; ns, not significant). Similar results were obtained for botulinum neurotoxin D light chain-expressing cells.

Δ C135 mKate2, was generated by producing an insert from nucleotides 2129–3459 and cloning this into the CAPS-mKate2 vector using *ScaI* and *EcoRI*. The forward primer was TAGACGAGTACTGCGCTCGGAATGGAGTCCGAGGATG, and the reverse primer was ACATGGAATTCCTTAGATGCCGCCTTCACCGTAAA. Rescue mutations were not needed in this vector because the target site lies within the deleted region.

Cell culture and transfections

PC12 cells were cultured in DMEM supplemented with 5% calf serum and 5% horse serum. Cells (6.25×10^6) were transfected by electroporation in a 2-mm-gap cuvette using an Electroporator II (Invitrogen, Carlsbad, CA) set at 71 μ F and 330 V. Transfections were done in cytomix (25 mM 4-(2-hydroxyethyl)-1-piperazineethanesulfonic acid [HEPES], pH 7.6, 120 mM KCl, 10 mM KH_2PO_4 , 0.15 mM

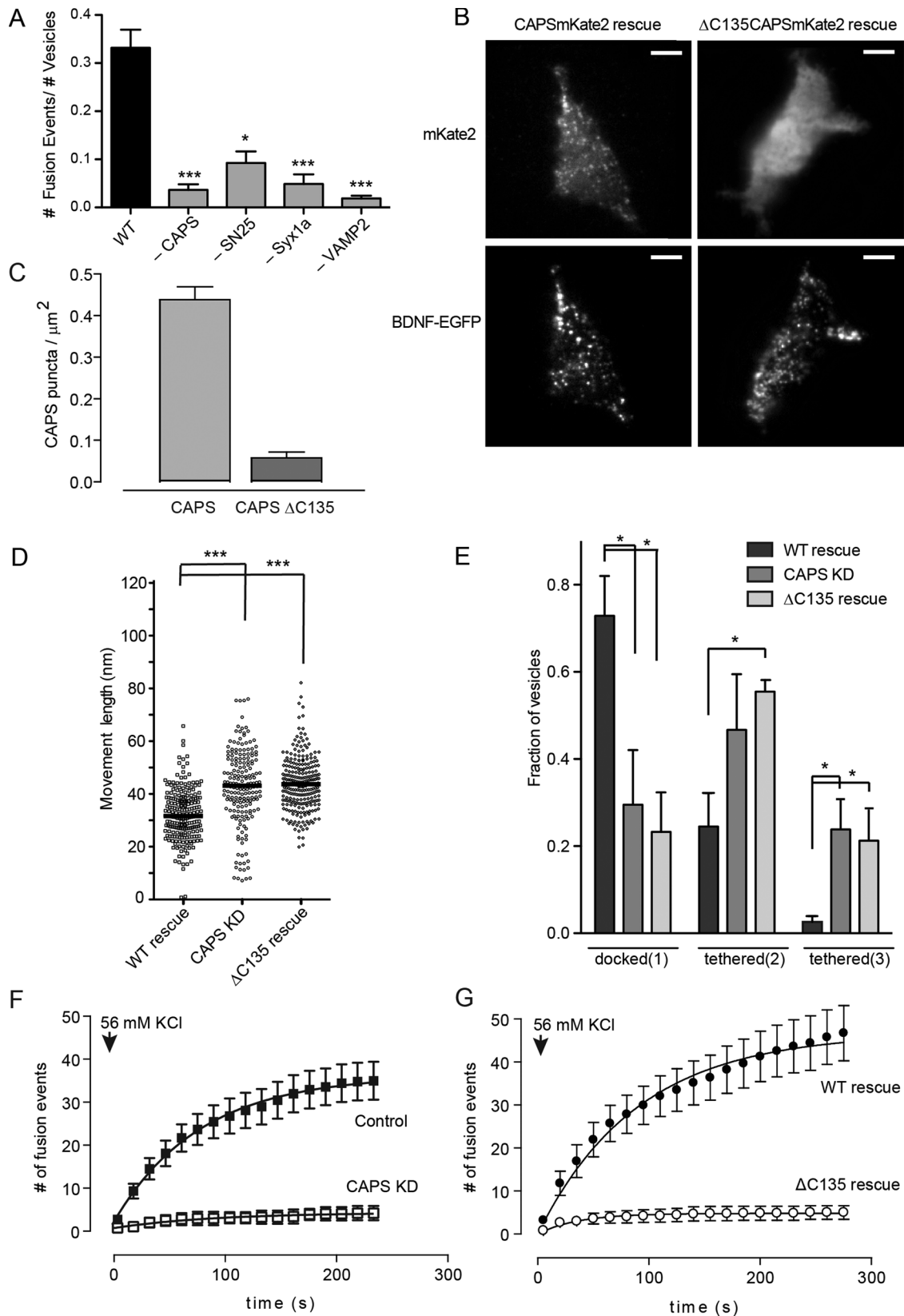


FIGURE 7: CAPS localization on DCVs is required for function. (A) Fusion probabilities (number of exocytic events/number of attached DCVs) were assessed with 56 mM KCl stimulation in cells knocked down for CAPS, SNAP-25, syntaxin-1, or VAMP-2 (means \pm SE, $n \geq 6$ cells; * $p < 0.01$, *** $p < 0.001$ compared with wild type). (B) TIRF images of live CAPS knockdown PC12 cells reexpressing either wild-type CAPS-mKate2 or CAPS(Δ C135)-mKate2 (top). BDNF-EGFP was coexpressed in the cells to monitor DCV distribution (bottom). Scale bar, 5 μm . (C) Average CAPS cluster density quantitated for wild-type CAPS- or CAPS(Δ C135)-expressing cells. (D) Scatterplot of attached DCV z-movement length

CaCl₂, 5 mM MgCl₂, 2 mM ATP, and 2 mM ethylene glycol tetraacetic acid) using 2–20 µg of DNA. HEK293FT cells (Invitrogen) were cultured in DMEM with high glucose and supplemented with 10% fetal bovine serum. A calcium phosphate protocol was used to transfect HEK cells at 70% confluency. DNA (20 µg) was diluted into 500 µl of a 250 mM CaCl₂ solution. This was added dropwise into 500 µl of bubbling 2× HeBS (280 mM NaCl, 1.5 mM Na₂HPO₄, and 50 mM HEPES at pH 7.05). After a 20-min incubation at room temperature, the precipitates were added to the cells in a dropwise manner. Cells were harvested 48 h posttransfection.

Live cells were imaged in basal buffer PSS-Na, (145 mM NaCl, 5.6 mM KCl, 2.2 mM CaCl₂, 0.5 mM MgCl₂, 15.0 mM HEPES, 5.6 mM glucose, pH 7.4). Potassium depolarization was achieved by switching the buffer to PSS-K (95 mM NaCl, 56 mM KCl, 2.2 mM CaCl₂, 0.5 mM MgCl₂, 15.0 mM HEPES, 5.6 mM glucose, pH 7.4) or to a similar 56 mM NaCl/95 mM KCl buffer as indicated. Actin disassembly was promoted by halichondramide (a kind gift from V. A. Klenchin, University of Wisconsin, Madison, WI) used at final concentration of 10 µM for 10 min diluted in PSS-Na (Klenchin *et al.*, 2003).

Immunofluorescence and Western blotting

Immunofluorescence studies for CAPS used a commercial CAPS polyclonal antibody (MyBioSource, San Diego, CA) and a chromogranin B monoclonal generously provided by W. B. Huttner (Max Planck Institute of Molecular Cell Biology and Genetics, Dresden, Germany). PC12 cells were permeabilized with 20 µM digitonin in a 4-min incubation before fixation in 4% paraformaldehyde, followed by 0.5% Triton X-100 extraction. Fixed cells were incubated with primary antibodies (1:50 dilution) for 2 h and with secondary antibodies for 1 h at room temperature. Z-stacks were obtained on a Nikon A1R confocal. For quantitating protein knockdown, cells that were mock transfected, transfected with shRNA plasmids, or expressing neurotoxin light chain constructs were immunostained, and fluorescence intensity per cell was measured. Measured fluorescence intensities were used to calculate percent knockdown. Cells were washed with phosphate-buffered saline (PBS), fixed with 4% paraformaldehyde (wt/vol), permeabilized in PBS containing 0.2% Triton X-100, and blocked in 10% fetal bovine serum (FBS) in PBS. Cells were incubated with primary antibody diluted in 10% FBS in PBS for 1 h at room temperature. Primary antibodies used were anti-syntaxin-1 monoclonal (HPC-1; Sigma-Aldrich, St. Louis, MO), anti-SNAP-25 polyclonal (LS-C10248; Lifespan Biochemicals, Seattle, WA), and anti-SNAP-25 monoclonal (SMI 81; Covance, Dedham, MA). After washing with PBS, cells were incubated with Alexa Fluor-conjugated secondary antibody for 1 h, washed, and imaged. To detect actin, we used phalloidin staining by fixing and extracting cells for incubation with Alexa Fluor 568-phalloidin (Molecular Probes, Eugene, OR) diluted 1:50 in blocking buffer for 30 min at room temperature and extensively washed with PBS.

Cell lysates from each condition were fractionated by SDS-PAGE for Western blotting. Proteins were transferred to nitrocellulose, washed, and blocked in 5% milk in PBS-Tween. Membranes were probed with the primary antibody for 1 h at room temperature and washed. Antibodies used for Western blotting were anti-syntaxin-

1A HPC-1 monoclonal (Sigma-Aldrich), anti-synaptobrevin2/VAMP2 polyclonal (raised against residues 2–17; Synaptic Systems, Goettingen, Germany), anti-SNAP-25 polyclonal (LS-C10248; Lifespan Biochemicals), anti-glyceraldehyde-3-phosphate dehydrogenase monoclonal (Ambion/Life Technologies, Grand Island, NY), and anti-CAPS polyclonal, which was generated against full-length purified rat CAPS protein. Horseradish peroxidase-conjugated secondary antibody was incubated with the membrane for 1 h at room temperature. Blots were exposed to film, and signals were quantified using a densitometer.

Single-molecule fluorescence

DNA encoding CAPS as mKate2-tagged proteins was transfected into HEK 293 cells as described. Cells were harvested 48 h after transfection, resuspended in 100 µl of PSS Na⁺, broken by two rounds of freeze-thaw, and pelleted at 14,000 rpm in a microcentrifuge at 4°C for 20 min. The supernatant was removed as cell lysate. Fluorescent protein concentrations were ~5 µM. For imaging single molecules, the cell lysates were diluted 1:250,000 into PSS Na⁺ and plated onto 35-mm glass-bottom dishes (MatTek, Ashland, MA). After a 5-min incubation, the dishes were washed with PSS Na⁺ to remove nonabsorbed molecules. Single fluorescently labeled molecules were imaged by TIRF using an Evolve Digital Monochrome electron-multiplying (EM) charge-coupled device (CCD) camera in photon counting mode (Photometrics, Tucson, AZ; Figure 3E). We sampled many of the molecules to demonstrate that most (>90%) exhibited single-step photobleach (Figure 3F). We then determined the average integrated fluorescence intensity of a single CAPS mKate2 molecule within an ROI of 0.8 µm² and subtracted the average background in same-size ROIs (Figure 3G). The mean value determined by a single Gaussian fit (*R*-square = 0.91) was 89 photons with SD of 60. We determined the average integrated fluorescence intensity of individual CAPS-mKate2 clusters in cells in the same size ROI (0.8 µm²) and performed a local average background subtraction for each cluster analyzed (Figure 3H). The mean value for this Gaussian fit (*R*-square = 0.95) was ~800 photons. The photon distribution of clusters was divided by the mean of the single-molecule standard to derive ~9 molecules of CAPS/per cluster (Figure 3H). Estimates of CAPS molecules/cluster were similar over a 2.5-fold range of CAPS-mKate2 expression. Images were analyzed using MetaMorph imaging software (Molecular Devices, Sunnyvale, CA), and data were fitted to a single-Gaussian distribution using Prism software.

TIRF microscopy

Cells were transfected and plated on 35-mm glass-bottom dishes (MatTek) coated with 0.1 mg/ml poly-DL-lysine and collagen (Sigma-Aldrich). After 72 h, cells were imaged on a Nikon TIRF Microscope Evanescent Wave Imaging System on a TE2000-U Inverted Microscope with an Apo TIRF 100×, numerical aperture (NA) 1.45 objective lens. EGFP fluorescence was excited with the 488-nm laser line of an argon ion laser. TagRFP, mKate2, and Alexa Fluor 568 fluorescence were excited with the 543-nm laser line of a HeNe laser. Simultaneous imaging from both lines was achieved using a Dual

for wild-type CAPS rescue (*n* = 487, median 31 nm), CAPS knockdown (*n* = 645, median 41 nm), and CAPS(ΔC135) rescue (*n* = 195, median 29 nm). Medians are indicated by black bar (***) *p* < 0.001). (E) The fraction of attached DCVs in pool 1 (docked), pool 2 (tethered), and pool 3 (tethered) for wild-type CAPS rescue, CAPS knockdown, or CAPS(ΔC135) rescue (mean values ± SE for *n* ≥ 10 cells; **p* < 0.01). (F) Time course of cumulative DCV exocytic events in control (black squares) and CAPS knockdown cells (white squares) after depolarization with 56 mM KCl. (G) Time course of cumulative DCV exocytic events in CAPS-knockdown cells expressing either wild-type CAPS (black circles) or CAPS(ΔC135) (open circles). Mean values ± SEM (*n* = 10–15 cells).

View imaging system (Optical Insights, Tucson, AZ). Images were acquired at 250-ms intervals with a CoolSNAP-ES Digital Monochrome CCD camera system (Photometrics) set to bin pixels 2×2 controlled by MetaMorph software or with an Evolve Digital Monochrome EM CCD camera system. Calibration of distance was performed under same 2×2 bin, which differs from calibrations reported previously (Lynch and Martin, 2007). Data analysis was done using MetaMorph software and FIJI (ImageJ; National Institutes of Health, Bethesda, MD). The TIRF microscope was calibrated to determine field penetration depth by the use of fluorescent beads. Fluorescent beads (0.05, 0.1, 0.2, 0.4, 0.5, or 1.0 μm in diameter) were absorbed to glass (MatTek) and imaged in PSS Na +15% BSA to mimic the refractive index of cytosol (1.35). Integrated intensities of beads were measured when the laser angle was set in the vertical position to illuminate entire sample (F_o). The laser angle was then set to achieve TIRF, and integrated intensity was measured (F). Curve fits of the F/F_o ratio, using an equation describing the exponentially weighted volume of a sphere to some height, calculated a decay constant ($1/e$) for our standard TIRF system of 160 nm.

Colocalization analysis

For colocalization analysis, we first defined a mask of the signal in either channel using the ImageJ tool Find Maxima and generated a mask using the output Maxima Within Tolerance that best described the signal. Colocalization within the regions specified by the independent masks of each channel was quantified using the Coloc 2 plug-in for Fiji for Figure 1. This program automates thresholding and reports statistically significant thresholded colocalization coefficients tM_1 and tM_2 as defined in Costes *et al.* (2004). We used the confined displacement algorithm (Ramirez *et al.*, 2010) implemented by the Genome Damage and Stability Centre (GDSC) plug-in for ImageJ by Alex Herbert (University of Sussex, Brighton, United Kingdom) for Figure 2, which calculates colocalization coefficients tM_1 and tM_2 for both channels following a pixel randomization assessment. These operations were applied to deconvolved images of confocal z-stacks obtained using Nikon A1 confocal microscope running Nikon Elements software.

Attached vesicle analysis

We defined vesicles belonging to the mobile pool when a vesicle moved at least 1 pixel or moved into or out of the TIRF field in 10 s. In our system, the average rate of transport was $110 \times 10^{-4} \mu\text{m}^2/\text{s}$ (1 pixel in 1.5 s), which is consistent with previously reported rates (Lang *et al.*, 2000). Vesicles were considered immobile if they moved <1 pixel in 10 s. However, on average, immobile vesicles moved at speeds of $<3 \times 10^{-4} \mu\text{m}^2/\text{s}$, which equates to 1 pixel every 60 s. Images were streamed at 4 Hz for 10 s. The resulting stack was processed into a single image to remove mobile vesicles, using stack arithmetic minimization. The minimized image was corrected for background. Individual vesicles were counted using either the Count Nuclei function in MetaMorph (method 1) or the Find Maxima function in FIJI (method 2). In addition, images were processed by a Top Hat morphology filter to separate vesicle clusters in method 1. Vesicle densities are reported as a function of the cell footprint membrane area. Method 2 resulted in lower total vesicle densities, but trends remained the same (unpublished data). Quantitation was done using only method 1 or 2 and reported with concomitant control cells.

The z-movement length analysis

All z-movement length image analysis was carried out in FIJI (ImageJ). Vesicles were identified using Find Maxima from an inten-

sity-minimized image from stacks streamed at 4 Hz for 7.5 s (30 frames). Points identified were used to create a binary mask. Mask points were dilated to encompass the entire vesicle. Isolated ROIs were selected for analysis to minimize contributions from neighboring vesicles. ROIs were transferred to the original stack (background corrected), and integrated intensity was monitored over time for each ROI. Maximum and minimum intensities for each ROI were found over a 7.5-s time period. Further increasing this sampling interval to 10–20 s did not affect the results. To determine maximum z-movement length from fluorescence changes, we used the equation $z(t) = -\lambda \ln(I_t/I_o)$, where $z(t)$ is maximum z-movement length, λ is $1/e$ of the evanescent field (160 nm), I_t is the minimum intensity, and I_o is the maximum intensity. The population of maximal vesicle z-movement lengths was plotted as a frequency plot (5-nm intervals), which was best fitted to a mix of three Gaussian distributions (adjusted R -square = 0.99). A model with four populations did not improve the adjusted R -square value, and a model with two populations reduced it. To distinguish changes in vesicle tether lengths, we used the intersections of the Gaussian curves (37 and 52 nm) to pool the data. The resolution of the z-measurement depends on the noise within the imaging system. We measured the z-movement of 100-nm beads adsorbed onto glass to assess this noise. Bead movements were distributed into a single-Gaussian population with mean centered at 27 nm (adjusted R -square = 0.985). The SD of the Gaussian fit was 6.8 nm, representing the precision of the measurement.

Variable-angle TIRF microscopy

Cells were transfected and plated on 35-mm glass-bottom dishes (MatTek) coated with 0.1 mg/ml poly-DL-lysine (Sigma-Aldrich). After 72–96 h, cells were imaged on a Nikon N-STORM Imaging System with an Apo TIRF 100 \times /NA 1.49 objective lens. EGFP fluorescence was excited with a 488-nm diode laser. The laser angle was set using a motorized TIRF illuminator programmed through Elements imaging software. Images were captured sequentially with 100-ms exposures using an iXon DU897 EM CCD camera (Andor, Concord, MA). We calculated the TIRF field penetration depth using the equation $d = \lambda/[4\pi(n_1^2 \sin^2\Theta - n_2^2)^{1/2}]$, where $\sin \Theta = 2rm/200,000n_1$, r is the distance of the laser illumination position from the center (in micrometers), n_1 and n_2 are the refractive indices of the glass and medium, respectively, and m is the magnification of the objective; TIRF angle positions (r) were found relative to the critical angle. The position illuminator angle used in live cells was calculated at a $1/e$ value of 90, 130, and >130 nm. These penetration depths were confirmed using fluorescent beads (0.05, 0.1, 0.2, and 0.4- μm diameter) absorbed to glass (MatTek) and imaged in PSS-Na plus 15% BSA. Bead images were obtained with the laser illuminator at 90, 130, >130 , or vertical positions. Total fluorescence (vertical position) was compared with bead fluorescence at each position. Total fluorescence of 0.05- and 0.1- μm beads was evident at ≥ 90 nm, whereas total fluorescence of the 0.2- μm bead was evident at ≥ 130 nm.

Variable-angle DCV density analysis

Images were streamed at 4 Hz for 7.5 s. The resulting stack was processed into a single image to remove mobile vesicles using stack arithmetic minimization. Mobile vesicles are defined as vesicles that moved in the xy - or z -dimension out of the TIRF field. At shallow angles, tethered vesicles moved out of the TIRF field and were considered “mobile” and were removed from density determinations. The minimized image was corrected for background. Individual vesicles were identified using the Find Maxima function in FIJI.

The noise tolerance was adjusted to the local background within the individual cell.

Statistical analysis

All statistical analysis was done using GraphPad Prism software, with the exception of Gaussian fitting, which was conducted in Matlab. A Mann–Whitney test for ANOVA was used to determine statistical significance between treatment groups of movement-length scatter plots, vesicle density, and fusion probabilities. Means of vesicle movement lengths were also subjected to two-way ANOVA analysis. Error bars are SEM.

ACKNOWLEDGMENTS

We thank Corinne Vokoun for her expertise in mixed Gaussian analysis and acknowledge the contributions of M. Petrie to early stages of the work. This work was supported by National Institutes of Health Grants DK040428 and DK025861 (to T.F.J.M.).

REFERENCES

- Aikawa Y, Lynch KL, Boswell KL, Martin TF (2006). A second SNARE role for exocytic SNAP25 in endosome fusion. *Mol Biol Cell* 17, 2113–2124.
- An SJ, Grabner CP, Zenisek D (2010). Real-time visualization of complexin during single exocytic events. *Nat Neurosci* 13, 577–583.
- Ann K, Kowalchuk JA, Loyet KM, Martin TF (1997). Novel Ca²⁺-binding protein (CAPS) related to UNC-31 required for Ca²⁺-activated exocytosis. *J Biol Chem* 272, 19637–19640.
- Arunachalam L, Han L, Tassew NG, He Y, Wang L, Xie L, Fujita Y, Kwan E, Davletov B, Monnier PP, et al. (2008). Munc18-1 is critical for plasma membrane localization of syntaxin1 but not of SNAP-25 in PC12 cells. *Mol Biol Cell* 19, 722–734.
- Barg S, Knowles MK, Chen X, Midorikawa M, Almers W (2010). Syntaxin clusters assemble reversibly at sites of secretory granules in live cells. *Proc Natl Acad Sci USA* 107, 20804–20809.
- Berwin B, Floor E, Martin TF (1998). CAPS (mammalian UNC-31) protein localizes to membranes involved in dense-core vesicle exocytosis. *Neuron* 21, 137–145.
- Brunk I, Blex C, Speidel D, Brose N, Ahnert-Hilger G (2009). Ca²⁺-dependent activator proteins of secretion promote vesicular monoamine uptake. *J Biol Chem* 284, 1050–1056.
- Carr CM, Rizo J (2010). At the junction of SNARE and SM protein function. *Curr Opin Cell Biol* 22, 488–495.
- Coffman VC, Wu JQ (2014). Every laboratory with a fluorescence microscope should consider counting molecules. *Mol Biol Cell* 25, 1545–1548.
- Costes SV, Daelemans D, Cho EH, Dobbin Z, Pavlakis G, Lockett S (2004). Automatic and quantitative measurement of protein-protein colocalization in live cells. *Biophys J* 86, 3993–4003.
- Daily NJ, Boswell KL, James DJ, Martin TF (2010). Novel interactions of CAPS (Ca²⁺-dependent activator protein for secretion) with the three neuronal SNARE proteins required for vesicle fusion. *J Biol Chem* 285, 35320–35329.
- Farina M, van de Bospoort R, He E, Persoon CM, van Weering JR, Broeke JH, Verhage M, Toonen RF (2015). CAPS-1 promotes fusion competence of stationary dense-core vesicles in presynaptic terminals of mammalian neurons. *Elife* 4, doi: 10.7554/eLife.05438.
- Friedrich R, Gottfried I, Ashery U (2013). Munc13-1 translocates to the plasma membrane in a Doc2B- and calcium-dependent manner. *Front Endocrinol* 4, 119.
- Fujita Y, Xu A, Xie L, Arunachalam L, Chou TC, Jiang T, Chiew SK, Kourtesis J, Wang L, Gaisano HY, Sugita S (2007). Ca²⁺-dependent activator protein for secretion 1 is critical for constitutive and regulated exocytosis but not for loading of transmitters into dense core vesicles. *J Biol Chem* 282, 21392–21403.
- Gandasi NR, Barg S (2014). Contact-induced clustering of syntaxin and munc18 docks secretory granules at the exocytosis site. *Nat Commun* 5, 3914.
- Gomi H, Mizutani S, Kasai K, Itohara S, Izumi T (2005). Granuphilin molecularly docks insulin granules to the fusion machinery. *J Cell Biol* 171, 99–109.
- Grishanin RN, Klenchin VA, Loyet KM, Kowalchuk JA, Ann K, Martin TF (2002). Membrane association domains in Ca²⁺-dependent activator protein for secretion mediate plasma membrane and dense-core vesicle binding required for Ca²⁺-dependent exocytosis. *J Biol Chem* 277, 22025–22034.
- Grishanin RN, Kowalchuk JA, Klenchin VA, Ann K, Earles CA, Chapman ER, Gerona RR, Martin TF (2004). CAPS acts as a prefusion step in dense-core vesicle exocytosis as a PIP2 binding protein. *Neuron* 43, 551–562.
- Hammarlund M, Watanabe S, Schuske K, Jorgensen EM (2008). CAPS and syntaxin dock dense core vesicles to the plasma membrane in neurons. *J Cell Biol* 180, 483–491.
- Harata NC, Aravanis AM, Tsien RW (2006). Kiss-and-run and full-collapse fusion as modes of exo-endocytosis in neurosecretion. *J Neurochem* 97, 1546–1570.
- Hong W, Lev S (2014). Tethering the assembly of SNARE complexes. *Trends Cell Biol* 24, 35–43.
- Hugo S, Dembla E, Halimani M, Matti U, Rettig J, Becherer U (2013). Deciphering dead-end docking of large dense core vesicles in bovine chromaffin cells. *J Neurosci* 33, 17123–17137.
- Imig C, Min SW, Krinner S, Arancillo M, Rosenmund C, Sudhof TC, Rhee J, Brose N, Cooper BH (2014). The morphological and molecular nature of synaptic vesicle priming at presynaptic active zones. *Neuron* 84, 416–431.
- Jahn R, Fasshauer D (2012). Molecular machines governing exocytosis of synaptic vesicles. *Nature* 490, 201–207.
- James DJ, Khodthong C, Kowalchuk JA, Martin TF (2008). Phosphatidylinositol 4,5-bisphosphate regulates SNARE-dependent membrane fusion. *J Cell Biol* 182, 355–366.
- James DJ, Kowalchuk J, Daily N, Petrie M, Martin TF (2009). CAPS drives trans-SNARE complex formation and membrane fusion through syntaxin interactions. *Proc Natl Acad Sci USA* 106, 17308–17313.
- James DJ, Martin TF (2013). CAPS and Munc13: CATCHRs that SNARE vesicles. *Front Endocrinol* 4, 187.
- Jockusch WJ, Speidel D, Sigler A, Sorensen JB, Varoqueaux F, Rhee JS, Brose N (2007). CAPS-1 and CAPS-2 are essential synaptic vesicle priming proteins. *Cell* 131, 796–808.
- Kabachinski G, Yamaga M, Kielar-Grevstad DM, Bruinsma S, Martin TF (2014). CAPS and Munc13 utilize distinct PIP2-linked mechanisms to promote vesicle exocytosis. *Mol Biol Cell* 25, 508–521.
- Karatekin E, Di Giovanni J, Iborra C, Coleman J, O’Shaughnessy B, Seagar M, Rothman JE (2010). A fast, single-vesicle fusion assay mimics physiological SNARE requirements. *Proc Natl Acad Sci USA* 107, 3517–3521.
- Karatekin E, Tran VS, Huet S, Faget I, Cribier S, Henry JP (2008). A 20-nm step toward the cell membrane preceding exocytosis may correspond to docking of tethered granules. *Biophys J* 94, 2891–2905.
- Kasai H, Takahashi N, Tokumaru H (2012). Distinct initial SNARE configurations underlying the diversity of exocytosis. *Physiol Rev* 92, 1915–1964.
- Khodthong C, Kabachinski G, James DJ, Martin TF (2011). Munc13 homology domain-1 in CAPS/UNC31 mediates SNARE binding required for priming vesicle exocytosis. *Cell Metab* 14, 254–263.
- Klenchin VA, Allingham JS, King R, Tanaka J, Marriott G, Rayment I (2003). Trisoxazole macrolide toxins mimic the binding of actin-capping proteins to actin. *Nat Struct Biol* 10, 1058–1063.
- Knowles MK, Barg S, Wan L, Midorikawa M, Chen X, Almers W (2010). Single secretory granules of live cells recruit syntaxin-1 and synaptosomal associated protein 25 (SNAP-25) in large copy numbers. *Proc Natl Acad Sci USA* 107, 20810–20815.
- Lang T, Wacker I, Wunderlich I, Rohrbach A, Giese G, Soldati T, Almers W (2000). Role of actin cortex in the subplasmalemmal transport of secretory granules in PC-12 cells. *Biophys J* 78, 2863–2877.
- Larson BT, Sochacki KA, Kindem JM, Taraska JW (2014). Systematic spatial mapping of proteins at exocytic and endocytic structures. *Mol Biol Cell* 25, 2084–2093.
- Lin XG, Ming M, Chen MR, Niu WP, Zhang YD, Liu B, Jiu YM, Yu JW, Xu T, Wu ZX (2010). UNC-31/CAPS docks and primes dense core vesicles in *C. elegans* neurons. *Biochem Biophys Res Commun* 397, 526–531.
- Liu Y, Schirra C, Stevens DR, Matti U, Speidel D, Hof D, Bruns D, Brose N, Rettig J (2008). CAPS facilitates filling of the rapidly releasable pool of large dense-core vesicles. *J Neurosci* 28, 5594–5601.
- Llobet A, Wu M, Lagnado L (2008). The mouth of a dense-core vesicle opens and closes in a concerted action regulated by calcium and amphiphysin. *J Cell Biol* 182, 1017–1028.
- Lynch KL, Martin TF (2007). Synaptotagmins I and IX function redundantly in regulated exocytosis but not endocytosis in PC12 cells. *J Cell Sci* 120, 617–627.

- MacDonald PE, Braun M, Galvanovskis J, Rorsman P (2006). Release of small transmitters through kiss-and-run fusion pores in rat pancreatic beta cells. *Cell Metab* 4, 283–290.
- Malsam J, Kreye S, Sollner TH (2008). Membrane fusion: SNAREs and regulation. *Cell Mol Life Sci* 65, 2814–2832.
- Martin TF, Kowalchuk JA (1997). Docked secretory vesicles undergo Ca²⁺-activated exocytosis in a cell-free system. *J Biol Chem* 272, 14447–14453.
- Mohrmann R, de Wit H, Connell E, Pinheiro PS, Leese C, Bruns D, Davletov B, Verhage M, Sorensen JB (2013). Synaptotagmin interaction with SNAP-25 governs vesicle docking, priming, and fusion triggering. *J Neurosci* 33, 14417–14430.
- Nofal S, Becherer U, Hof D, Matti U, Rettig J (2007). Primed vesicles can be distinguished from docked vesicles by analyzing their mobility. *J Neurosci* 27, 1386–1395.
- Nojiri M, Loyet KM, Klenchin VA, Kabachinski G, Martin TF (2009). CAPS activity in priming vesicle exocytosis requires CK2 phosphorylation. *J Biol Chem* 284, 18707–18714.
- Paddison PJ, Cleary M, Silva JM, Chang K, Sheth N, Sachidanandam R, Hannon GJ (2004). Cloning of short hairpin RNAs for gene knockdown in mammalian cells. *Nat Methods* 1, 163–167.
- Renden R, Berwin B, Davis W, Ann K, Chin CT, Kreber R, Ganetzky B, Martin TF, Broadie K (2001). Drosophila CAPS is an essential gene that regulates dense-core vesicle release and synaptic vesicle fusion. *Neuron* 31, 421–437.
- Rizo J, Sudhof TC (2012). The membrane fusion enigma: SNAREs, Sec1/Munc18 proteins, and their accomplices—guilty as charged? *Annu Rev Cell Dev Biol* 28, 279–308.
- Sadakata T, Kakegawa W, Shinoda Y, Hosono M, Katoh-Semba R, Sekine Y, Sato Y, Tanaka M, Iwasato T, Itoharu S, et al. (2013). CAPS1 deficiency perturbs dense-core vesicle trafficking and Golgi structure and reduces presynaptic release probability in the mouse brain. *J Neurosci* 33, 17326–17334.
- Shi L, Shen QT, Kiel A, Wang J, Wang HW, Melia TJ, Rothman JE, Pincet F (2012). SNARE proteins: one to fuse and three to keep the nascent fusion pore open. *Science* 335, 1355–1359.
- Shinoda Y, Sadakata T, Nakao K, Katoh-Semba R, Kinameri E, Furuya A, Yanagawa Y, Hirase H, Furuichi T (2011). Calcium-dependent activator protein for secretion 2 (CAPS2) promotes BDNF secretion and is critical for the development of GABAergic interneuron network. *Proc Natl Acad Sci USA* 108, 373–378.
- Sieber JJ, Willig KI, Kutzner C, Gerding-Reimers C, Harke B, Donnert G, Rammner B, Eggeling C, Hell SW, Grubmuller H, Lang T (2007). Anatomy and dynamics of a supramolecular membrane protein cluster. *Science* 317, 1072–1076.
- Smyth AM, Rickman C, Duncan RR (2010). Vesicle fusion probability is determined by the specific interactions of munc18. *J Biol Chem* 285, 38141–38148.
- Smyth AM, Yang L, Martin KJ, Hamilton C, Lu W, Cousin MA, Rickman C, Duncan RR (2013). Munc18-1 protein molecules move between membrane molecular depots distinct from vesicle docking sites. *J Biol Chem* 288, 5102–5113.
- Sollner T, Whiteheart SW, Brunner M, Erdjument-Bromage H, Geromanos S, Tempst P, Rothman JE (1993). SNAP receptors implicated in vesicle targeting and fusion. *Nature* 362, 318–324.
- Sorensen JB, Wiederhold K, Muller EM, Milosevic I, Nagy G, de Groot BL, Grubmuller H, Fasshauer D (2006). Sequential N- to C-terminal SNARE complex assembly drives priming and fusion of secretory vesicles. *EMBO J* 25, 955–966.
- Speese S, Petrie M, Schuske K, Ailion M, Ann K, Iwasaki K, Jorgensen EM, Martin TF (2007). UNC-31 (CAPS) is required for dense-core vesicle but not synaptic vesicle exocytosis in *Caenorhabditis elegans*. *J Neurosci* 27, 6150–6162.
- Speidel D, Bruederle CE, Enk C, Voets T, Varoqueaux F, Reim K, Becherer U, Fornai F, Ruggieri S, Holighaus Y, et al. (2005). CAPS1 regulates catecholamine loading of large dense-core vesicles. *Neuron* 46, 75–88.
- Speidel D, Salehi A, Obermueller S, Lundquist I, Brose N, Renstrom E, Rorsman P (2008). CAPS1 and CAPS2 regulate stability and recruitment of insulin granules in mouse pancreatic beta cells. *Cell Metab* 7, 57–67.
- Steyer JA, Almers W (2001). A real-time view of life within 100 nm of the plasma membrane. *Nat Rev Mol Cell Biol* 2, 268–275.
- Sudhof TC, Rothman JE (2009). Membrane fusion: grappling with SNARE and SM proteins. *Science* 323, 474–477.
- Takahashi N, Hatakeyama H, Okado H, Noguchi J, Ohno M, Kasai H (2010). SNARE conformational changes that prepare vesicles for exocytosis. *Cell Metab* 12, 19–29.
- Taraska JW, Perras I, Ohara-Imaizumi M, Nagamatsu S, Almers W (2003). Secretory granules are recaptured largely intact after stimulated exocytosis in cultured endocrine cells. *Proc Natl Acad Sci USA* 100, 2070–2075.
- Toonen RF, Kochubey O, de Wit H, Gulyas-Kovacs A, Konijnenburg B, Sorensen JB, Klingauf J, Verhage M (2006). Dissecting docking and tethering of secretory vesicles at the target membrane. *EMBO J* 25, 3725–3737.
- Tsuboi T, Fukuda M (2005). The C2B domain of rabphilin directly interacts with SNAP-25 and regulates the docking step of dense core vesicle exocytosis in PC12 cells. *J Biol Chem* 280, 39253–39259.
- Tsuboi T, Fukuda M (2006). The Slp4-a linker domain controls exocytosis through interaction with Munc18-1/syntaxin-1a complex. *Mol Biol Cell* 17, 2101–2112.
- van den Bogaart G, Holt MG, Bunt G, Riedel D, Wouters FS, Jahn R (2010). One SNARE complex is sufficient for membrane fusion. *Nat Struct Mol Biol* 17, 358–364.
- Verhage M, Sorensen JB (2008). Vesicle docking in regulated exocytosis. *Traffic* 9, 1414–1424.
- Walent JH, Porter BW, Martin TF (1992). A novel 145 kd brain cytosolic protein reconstitutes Ca²⁺-regulated secretion in permeable neuroendocrine cells. *Cell* 70, 765–775.
- Wang CT, Lu JC, Bai J, Chang PY, Martin TF, Chapman ER, Jackson MB (2003). Different domains of synaptotagmin control the choice between kiss-and-run and full fusion. *Nature* 424, 943–947.
- Weber T, Zemelman BV, McNew JA, Westermann B, Gmachl M, Parlati F, Sollner TH, Rothman JE (1998). SNAREpins: minimal machinery for membrane fusion. *Cell* 92, 759–772.
- Weninger K, Bowen ME, Choi UB, Chu S, Brunger AT (2008). Accessory proteins stabilize the acceptor complex for synaptobrevin, the 1:1 syntaxin/SNAP-25 complex. *Structure* 16, 308–320.
- Wojcik SM, Brose N (2007). Regulation of membrane fusion in synaptic excitation-secretion coupling: speed and accuracy matter. *Neuron* 55, 11–24.
- Wu Y, Gu Y, Morpheus MK, Yao J, Yeh FL, Dong M, Chapman ER (2012). All three components of the neuronal SNARE complex contribute to secretory vesicle docking. *J Cell Biol* 198, 323–330.
- Xia X, Lessmann V, Martin TF (2009). Imaging of evoked dense-core-vesicle exocytosis in hippocampal neurons reveals long latencies and kiss-and-run fusion events. *J Cell Sci* 122, 75–82.
- Xu T, Binz T, Niemann H, Neher E (1998). Multiple kinetic components of exocytosis distinguished by neurotoxin sensitivity. *Nat Neurosci* 1, 192–200.
- Yu IM, Hughson FM (2010). Tethering factors as organizers of intracellular vesicular traffic. *Annu Rev Cell Dev Biol* 26, 137–156.
- Zhang X, Kim-Miller MJ, Fukuda M, Kowalchuk JA, Martin TF (2002). Ca²⁺-dependent synaptotagmin binding to SNAP-25 is essential for Ca²⁺-triggered exocytosis. *Neuron* 34, 599–611.
- Zhou KM, Dong YM, Ge Q, Zhu D, Zhou W, Lin XG, Liang T, Wu ZX, Xu T (2007). PKA activation bypasses the requirement for UNC-31 in the docking of dense core vesicles from *C. elegans* neurons. *Neuron* 56, 657–669.
- Zilly FE, Sorensen JB, Jahn R, Lang T (2006). Munc18-bound syntaxin readily forms SNARE complexes with synaptobrevin in native plasma membranes. *PLoS Biol* 4, e330.